Heat and Mass Transfer in turbulent Taylor-Couette flows with an axial throughflow

Adrien Aubert, Sébastien Poncet, Patrice Le Gal, Stéphane Viazzo, Michael Le Bars, Thomas Thouveny

Heat and Mass Transfer in turbulent Taylor-Couette flows with an axial throughflow

A. Aubert[a,b], S. Poncet[b], P. Le Gal[a], S. Viazzo[b], M. Le Bars[a], T. Thouveny[a]

a. *Institut de Recherche sur les Phénomènes Hors Equilibre, Marseille*
b. *Laboratoire de Modélisation en Mécanique et Procédés Propres, Marseille*

Résumé :

On s'intéresse ici aux transferts de chaleur et de masse dans l'entrefer rotor-stator d'un moteur électrique modélisé par un système de Taylor-Couette avec flux axial. Un dispositif expérimental permettant des mesures de vitesse et de coefficient de transferts a été récemment développé. Les régimes étudiés sont turbulents avec des nombres de Reynolds axial Re et de Taylor Ta atteignant respectivement les valeurs 1.12×10^4 *et* 7.9×10^7*. Des mesures de vitesse par LDV, PIV et Stereo-PIV sont comparées en termes de champs moyen et turbulent. La présence de structures organisées proche du rotor a été observée expérimentalement et numériquement par DNS. Concernant le nombre de Nusselt, on montre que les valeurs mesurées varient en fonction du nombre de Taylor selon une loi d'échelle faisant intervenir l'épaisseur de la couche limite du rotor à la puissance* $-1/10$*.*

Abstract :

In the present work, we investigate the heat and mass transfer in the rotor-stator gap of an electrical motor modeled by a Taylor-Poiseuille system with an axial throughflow. An experimental set-up has been recently developed and enables to perform velocity and heat transfer measurements. The axial Reynolds number Re and the Taylor number Ta reach the values 1.12×10^4 *and* 7.9×10^7 *respectively so that the flow is turbulent. Velocity measurements are performed by LDV, PIV and Stereo-PIV. They highlight in particular the presence of coherent structures within the rotor boundary layer, which is confirmed by a DNS calculation. The measured values of the Nusselt number are found to be proportional to the rotor boundary layer thickness to the power* $-1/10$*.*

Mots clefs : Taylor-Couette-Poiseuille flow ; heat transfer ; turbulent flow

1 Introduction

Though Taylor-Couette flows with or without an axial throughflow have been already widely considered over the last decades, Fénot et *al.* [2] showed in their recent review paper that there are still some unresolved issues especially about the distribution of the heat transfer coefficient. If Gilchrist et *al.* [3] observed only a weak influence of the axial Reynolds number, other authors like Bouafia et *al.* [1] proposed correlations depending on both the Taylor and Reynolds numbers. Several reasons may be invoked to explain the dispersion of the collected data : the different ranges of flow control parameters (axial inlet velocity and rotation rate) and the size of the systems considered. In some correlations synthetized by [2], the authors considered too short cavities to get a fully developed flow. In that cases, correlations for the Nusselt number appear to be strongly dependent on the inlet conditions.

This type of flow is encountered in various industrial applications. The direct application of the present paper is the effective cooling of the rotor-stator gap of an electrical motor, which is actually not optimum in the real machinery. An experimental set-up has been then recently designed to investigate the heat transfer process preserving the same geometry in terms of aspect and radius ratios as in the turbopump. However, instead of using air as in real rotating machineries, water has been chosen as

the working fluid enabling to consider lowest rotation rates while preserving the similarity parameters (Rossby and Reynolds numbers). The aim is to bring a better insight into the understanding of the heat and mass transfer mechanisms within the rotor-stator gap in the turbulent regime.

2 Experimental set-up and measurement techniques

2.1 General description and flow parameters

The system (Fig.1) is composed of two concentric cylinders of length $L = 0.5$ m. The inner cylinder of radius $R_i = 8$ cm rotates around its axis at the rate Ω. The outer cylinder of radius $R_o = 9$ cm is stationary. It is made of PMMA to allow optical velocimetry techniques. Both cylinders are located in a tank made of PMMA that is regulated in temperature by a refrigerated circulator. The axial volumetric flow rate Q is imposed within the gap $e = R_o - R_i = 1$ cm by a centrifugal pump from the top to the bottom. Before entering the rotor-stator cavity, the water flow coming from 6 pipes is collected in a small cavity. When leaving the gap, water is gathered in an open tank which is also regulated in temperature. Water temperature is measured at the entrance and at the outlet of the gap through a set of 2 PT 100 probes located at 0.85 cm radius.

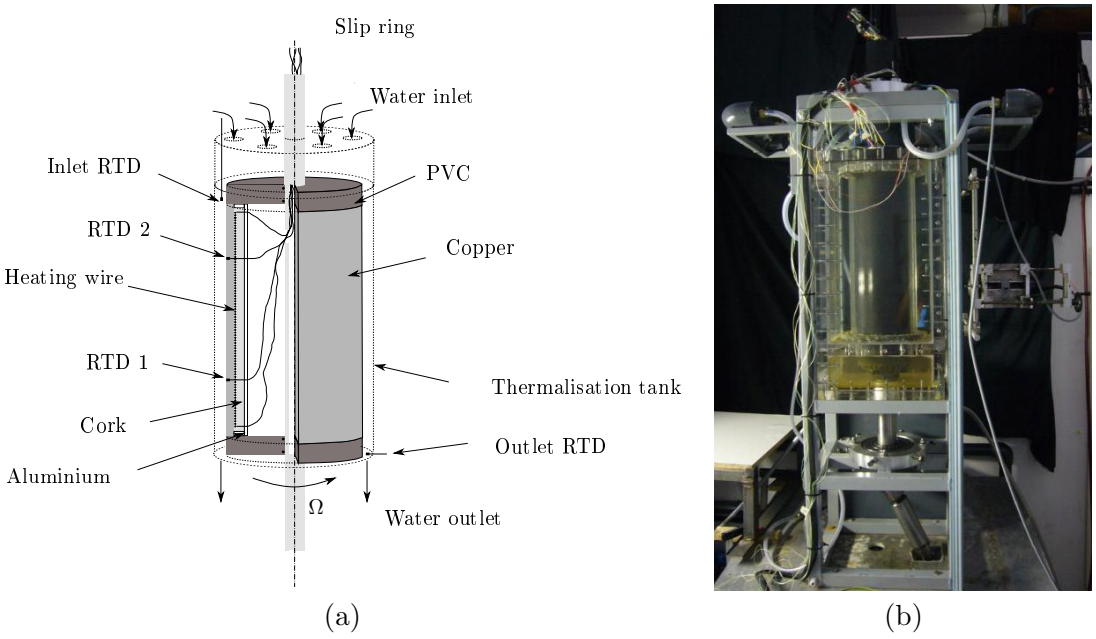

FIGURE 1 – (a) Schematic representation and (b) photograph of the experimental facility.

The cavity may be characterized by two geometrical parameters, its aspect ratio Γ and its radius ratio s. The hydrodynamic and thermal fields depend mainly on the axial Reynolds number Re, the Taylor Ta and Prandtl Pr numbers. They are all defined below :

$$\Gamma = \frac{L}{e} = 50 \qquad s = \frac{R_i}{R_o} = 0.89 \qquad Pr = \frac{\nu}{\alpha} = 6 \qquad Re = \frac{2V_{deb}e}{\nu} \qquad Ta = \frac{\Omega^2 R_i e^3}{\nu^2} \tag{1}$$

where $V_{deb} = Q/[\pi(R_o^2 - R_i^2)]$ is the axial velocity imposed at the inlet, α the thermal diffusivity of water and ν its kinematic viscosity.

2.2 Details about the rotor

The rotor, which is also dedicated to supply a heat flux of 4.9 kW/m^2 to the fluid, is itself made of two concentric cylinders. The inner one is a 6 cm radius tube in aluminium. A 1 cm layer of cork was

stuck on it to reduce heat losses. Then 60 m of a 4 mm diameter heating wire (1 Ω/m) was wound on the cork layer. Conductive silver paste was added to fill the gap between the rings. A 8 cm radius tube in copper (5 mm thickness) was threaded on this assembly. In order to close the rotor, two PVC end caps (5 cm thickness) were assembled on both sides. The motor shaft is a 3 cm radius tube in stainless steel metal. A small hole was drilled in it to take out every wires (probes and heating resistance) from the inner part of the rotor to a slip ring located at the top of the shaft. The shaft was passed through the end caps of the rotor and sealing was achieved by two O-rings on both sides. Pressure screws on the end caps allow a proper alignment (± 0.15 mm) and positioning of the cylinders respectively to the shaft. The rotor is mounted on 2 bearings. Atop, a lip seal is used for sealing between the shaft and the cavity as well as for the bottom.

To perform parietal temperature measurements, 4 RTD probes (PT100) were carefully incorporated in the rotor, such that they smoothly flush the outer surface. They were arranged in pairs symmetrically opposite respectively located at 16.7 and 33.3 cm from the top of the cylinder. Data were acquired using a 4 channel analog module.

2.3 Experimental procedure and data treatment

The axial w and azimuthal v component of the velocity vector are measured by a two-component LDV sytem arranged as shown in figure 2. Seeding was achieved with 5 μm polyamide particles. Each sample was conducted during 2 minutes in order to obtain a statistical convergence of the velocity.

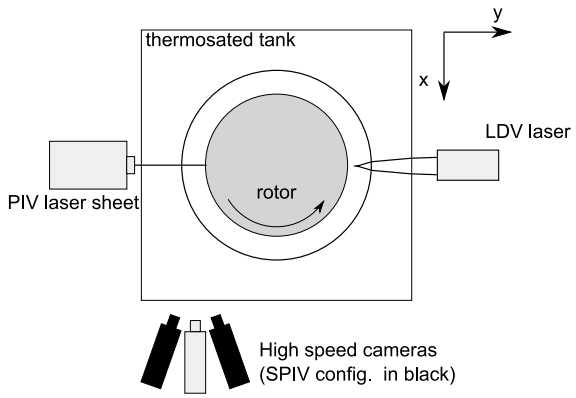

FIGURE 2 – Arrangement of the different velocity measurement systems.

PIV and SPIV (Stéréo-PIV) measurements were also performed by using a 5 W continuous laser and two high speed cameras. Data acquisition frequency is set at 1500 Hz for a 512x1024 pixels resolution. The camera buffer limits the acquisition time at 2.6 s. Polyamide particles of 30 μm in diameterwere used to seed the flow. Cross-correlation between the different frames are performed with DPIVSoft [4]. Interrogations windows are in the first run 64x64 pixels with 50 % overlapping. They are then translated and deformed according to the velocity field estimation. Smaller windows (32x32 pixels with 50 % overlapping) are then chosen to enhance the spatial resolution.

Axial components w and azimuthal components v are made dimensionless by dividing by the mean inlet axial velocity V_{deb} and the rotor wall velocity ΩR_i respectively. Thus $w* = w/V_{deb}$ and $v* = v/(\Omega R_i)$. The gap length is normalized to be equal to $e^* = 0$ on the rotor and 1 on the stator.

The experimental procedure for the temperature measurements is described as follows. At first, the different temperature regulation systems are switched on. The pump is also turned on and the gap is filled with water before starting the rotation of the inner cylinder. When the whole system reaches the thermal equilibrium, data acquisition is triggered. Finally, the heating wire is powered. Different experiments gave that around 2h30 are necessary for the system to reach the steady state. The temperature of the incoming fluid is then close to $25°C$. A 2D axisymmetric model developed with COMSOL

allowed to estimate the heat loss in our system considering mainly conductive transfers. The wall heat flux is found to be equal to 90% of the flux provided by the heating wire.

3 Results and discussion

3.1 Velocity measurements

Figures 3a and 3b compare the different velocity measurement techniques used here in terms of the mean axial $w*$ and tangential $v*$ components of the mean velocity vector for a given set of parameters : $Ta = 7.9 \times 10^7$ and $Re = 7490$. Measurements have been performed at 45 cm from the inlet ($\simeq 22$ hydraulic diameters), where the flow may be considered as established. The radial profiles of the axial velocity are rather the same whatever the technique used with a typical turbulent Poiseuille flow profile within the gap. The resolution within the boundary layers is lower because of laser reflections inducing a loss of information. There is also a good agreement for the azimuthal component in the central part of the gap, where v^* is almost constant with e^*. There is no experimental data available close to the walls because of experimental constraints.

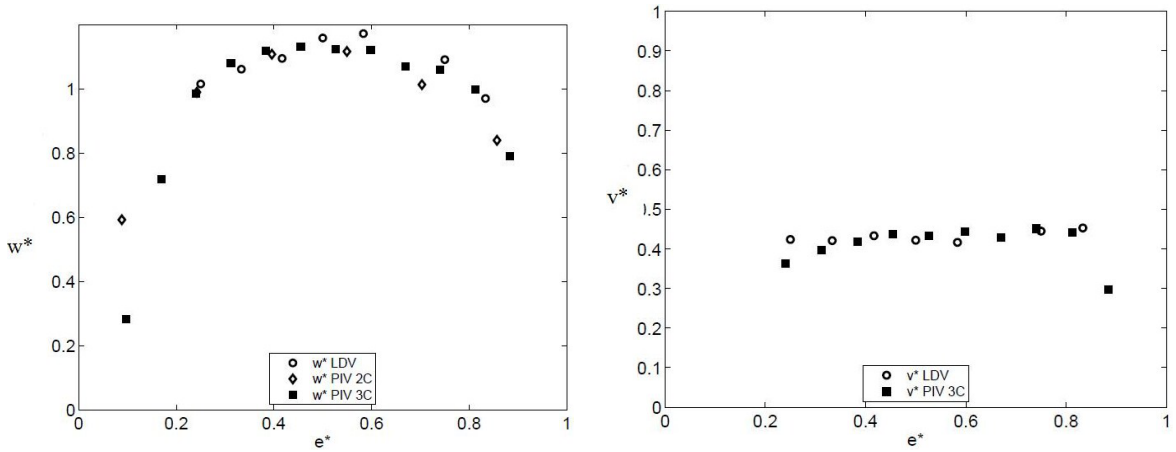

(a) (b)

FIGURE 3 – Radial profiles of the (a) axial and (b) azimuthal velocity components for $Ta = 7.9 \times 10^7$ and $Re = 7490$. Comparisons between the LDV, PIV and SPIV measurements.

The normal axial $< w >_{rms}$ and azimutal $< v >_{rms}$ components of the Reynolds stress tensor are shown in figure 4. There is a good agreement between the LDV and SPIV measurements for the axial component with maxima obtained close to the walls. Turbulence intensities are particularly high. For the azimuthal component, there are some discrepancies, which may be explained by the short acquisition time of the SPIV measurements and so by a lesser statistical convergence of the data.

The SPIV measurements have been performed at a sufficiently high frequency (1500 Hz) to be resolved in time and to make the Taylor hypothesis valid. By considering also that the flow is mainly in solid body rotation, we can calculate the λ_2 criterion, which is the second proper value of the $S^2 + A^2$ tensor, where S and A are the symmetric and antisymmetric parts of the velocity gradient tensor approximated using second order finite difference schemes. The isovalues of λ_2 enable to highlight the presence of coherent structures within the flow. One example is given in figure 5a for $Re = 7490$ and $Ta = 8.7 \times 10^6$. The axial fluid flows from the top to the bottom and time is increasing from the right to the left. Coherent structures along the rotor side can be observed with a given inclination angle. There is no apparent 3D large scale vortices within the core of the flow. These results are in qualitative good agreement with the iso-values of the Q criterion (Fig.5b) obtained by DNS (see in [5]).

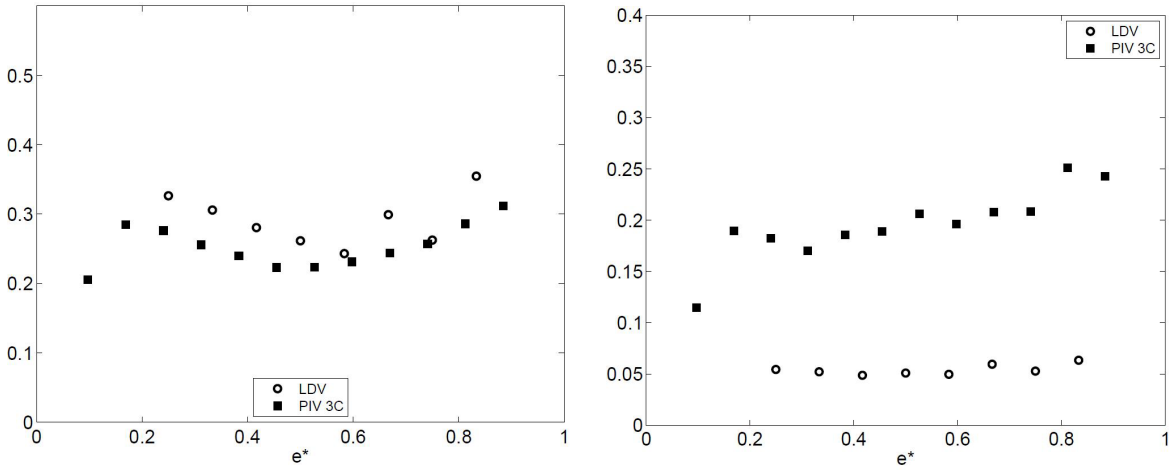

FIGURE 4 – Radial profiles of the (a) axial $< w >_{rms} /V_{deb}$ and (b) azimuthal $< v >_{rms} /(\Omega R_1)$ turbulence intensities for $Ta = 7.9 \times 10^7$ and $Re = 7490$.

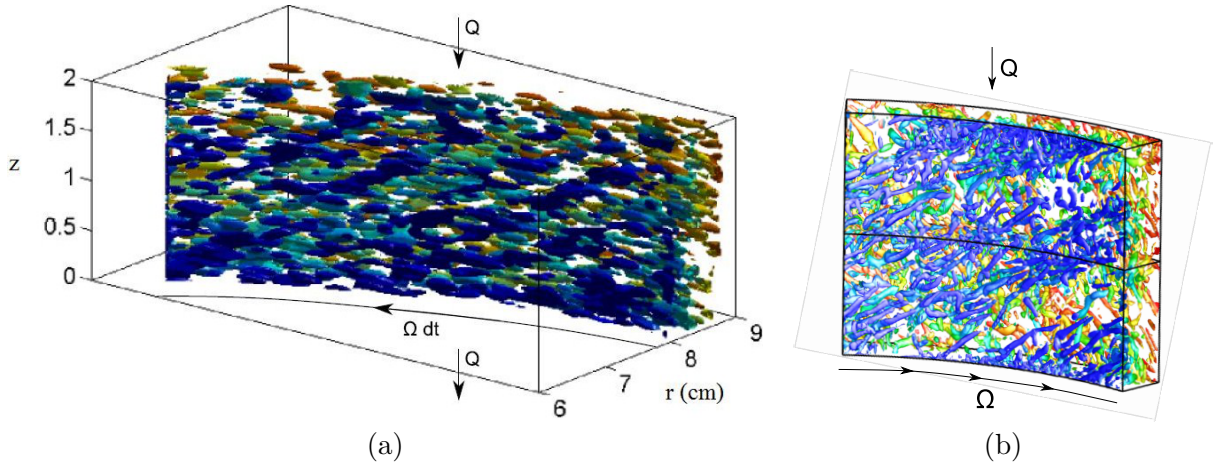

FIGURE 5 – Coherent structures : (a) $\lambda_2 = 10^3$ criterion obtained experimentally for $Re = 7490$ et $Ta = 8.7 \times 10^6$; (b) isovalues of the Q criterion obtained by DNS for $Re = 8 \times 10^3$ et $Ta = 2.6 \times 10^7$.

3.2 Heat transfer coefficient

Figure 6a presents the Nusselt number $Nu = he/\lambda$ (λ the thermal conductivity of water) on the rotor as a function of the Taylor number for $Re = 11200$. There is a noticeable difference between the values obtained with the upper and lower probes due to the transient nature of the heat transfer process. Nu is clearly an increasing function of Ta with more important variations for weak rotation rates. It may be attributed to the coherent structures observed within the rotor boundary layer, which would prevent the axial flow to cool the rotor at high rotation rates. Figure 6b compares the present results with the ones of [3]. Though the values of Re considered are somewhat different (ratio between 5 and 10), a good agreement is observed at high Ta values. At low rotation rates, differences are more important.

For rotating flows, the thickness of the Ekman boundary layer δ in the turbulent regime is found to be proportionnal to $(\nu/\Omega)^{1/5}$. If the heat transfer process is purely conductive, we get : $h = \lambda/\delta$. Finally, the Nusselt number can be expressed under the form : $Nu = Be\left(\frac{\Omega}{\nu}\right)^{1/5}$, with $B = 110$ for the upper probe and 60 for the lower one. These two scaling laws are plotted on Figures 6a and 6b.

For $Ta > 2 \times 10^7$, the scaling laws fit quite well the experimental results for both probes. At lowest values, the discrepancy is more noticeable. It was expected as at low Ta, the boundary layer which pilots the heat transfer process is the one due to the axial flow and not to the one due to rotation.

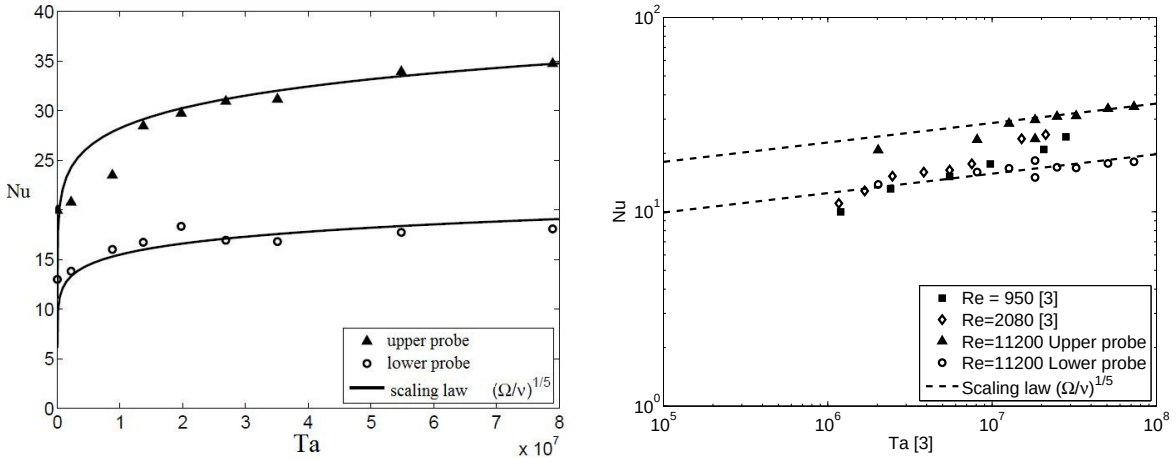

(a) (b)

FIGURE 6 – (a) Evolution of the Nusselt number according to the Taylor number for $Re = 11200$; (b) Comparison with the previous results of [3].

4 Conclusion

Though the Taylor-Couette-Poiseuille has already been widely considered over the last decades, the interaction between the axial flow used to cool the rotating inner cylinder and its rotation makes the hydrodynamic flow and heat transfer process highly complex. There is in particular a strong competition between the Ekman and Blasius boundary layers, which highlights a regime transition at a critical Taylor number. At low values of the Taylor number, the heat transfer coefficient on the rotor increases strongly with rotation, probably by destruction of the boundary layer. The rotation dominating regime prevents the axial flow to penetrate the rotor boundary layer in spite of the turbulent nature of the flow. It could explain while manufacturers have some problems to predict the good amount of coolant in real rotating machineries. Moreover, the transient nature of the flow induces large variations of the Nusselt number, which makes the use of previous data avalaible in the literature not so easy.

Références

[1] Bouafia M., Bertin Y., Saulnier J.B., Roper P. 1998 Analyse expérimentale des transferts de chaleur en espace annulaire étroit et rainuré avec cylindre intérieur tournant. *Int. J. Heat Mass Transfer* **41 (10)** 1279-1291

[2] Fénot M., Bertin Y., Dorignac E., Lalizel G. 2011 A review of heat transfer between concentric rotating cylinders with or without axial flow. *Int. J. Thermal Sci.* **50 (7)** 1138-1155

[3] Gilchrist S., Ching C.Y., Ewing D. 2005 Heat Transfer Enhancement in Axial Taylor-Couette Flow. *ASME Conference Proceedings* 227-233

[4] Meunier P., Leweke T. 2003 Analysis and minimization of errors due to high gradients in Particle Image Velocimetry. *Exp. Fluids* **35** 408-421

[5] Oguic, R., Viazzo, S., Poncet, S. 2013 Numerical simulations of a middle gap turbulent Taylor-Couette-Poiseuille flow. *Ercoftac workshop : Direct and Large-Eddy Simulation 9*, Dresden.